Liquid crystal polymer substrate MMIC receiver modules for the ECE Imaging system on the DIII-D[a)]

Y. Zhu[1,b)], Y. Ye[1], J-H. Yu[1], B. Tobias[2], A-V. Pham[1], Y. Wang[1], C. Luo[1], C. Domier[1], G. Kramer[3], Y. Ren[3], A. Diallo[3], N. Raffi[3], M. Chen[1], G. Yu[1], N.C. Luhmann[1]

[1]*University of California Davis, Davis, California, 95616, USA*
[2]*Los Alamos National Laboratory, New Mexico, 87545*
[3]*Princeton Plasma Physics Laboratory, Princeton, New Jersey 08543, USA*

(Presented XXXXX; received XXXXX; accepted XXXXX; published online XXXXX)
(Dates appearing here are provided by the Editorial Office)

A new generation of millimeter-wave heterodyne imaging receiver arrays has been developed and demonstrated on the DIII-D ECEI system. Improved circuit integration, allowing for absolute calibration, improved noise performance, and shielding from out-of-band emission, is made possible by using advanced liquid crystal polymer (LCP) substrates and MMIC (Monolithic Microwave Integrated Circuit) receiver chips. This array exhibits ~ 15 dB additional gain and > 30x reduction in noise temperature compared to the previous generation and provide ECEI capability for absolute 2-D electron temperature profile measurements. Each LCP horn-waveguide module houses a 3x3 mm GaAs MMIC receiver chip, which consists of a low noise amplifier (LNA), balanced mixer, local oscillator multiplier chain driven by ~12 GHz input via an RF cable to the enclosure box, and IF amplifier. A proof-of-principle instrument with 5 poloidal channels was installed on DIII-D in 2017. The full proof-of-principle system installation (20 poloidal x 8 radial channels) was commissioned early in 2018. The LCP ECEI system is used for pedestal region measurements, especially focusing on temperature evolution during ELM bursting. The DIII-D ECE Imaging signal has been significantly improved with extremely effective shielding of out-of-band microwave noise which plagued previous ECE Imaging studies on DIII-D. In H-mode ELM bursting, the radial propagation of electron heat flow has been detected on DIII-D. The LCP ECE Imaging is expected to be a valuable diagnostic tool for ELM physics investigations.

I. Introduction

The Electron Cyclotron Emission Imaging (ECE Imaging) diagnostic pioneered by UC Davis has been widely employed on many tokamaks[1,2,3,4,5,6,7] for 2D electron temperature fluctuation measurements by collecting spontaneous 2nd harmonic electron cyclotron emission. Over the past ten years, ECE Imaging has been employed as a powerful high-speed imaging diagnostic to capture multi-scale physics phenomena in the core and edge regions in the plasma, including the sawtooth crash[8], Alfven eignmodes[9], neoclassical tearing modes[10], and ELM filaments[11] The discovery of more elaborate structures requires the development of advanced diagnostic techniques, especially for the pedestal region confinement improvement.

Integrated circuit (IC) technology facilitates combining many bulky microwave components onto a tiny piece of the semiconductor substrate as a "system-on-chip" (SoC). It has been widely applied in wireless communication, sensitive radar on satellites, and cellular phones. Likewise, IC technology could bring transformative advances in millimeter-wave diagnostics for fusion plasmas[12]. Comparing with current technology, the IC approach could significantly improve the signal to noise ratio, which could provide possibilities for absolutely calibrated temperature imaging and high resolution measurement of turbulent spectra. With the new IC technology, the ECE Imaging system has the much stronger rejection of out-of-band interference and thus the receiving signal will be relatively immune from millimeter-wave bursting. In addition, the protection from strong RF heating and current drive system could increase diagnostic tolerance. In the new IC approach, the LO coupling is no longer via the use of quasi-Gaussian beams. Instead, the directly coupled microwave LO drive removes one possible path for interference while supporting stable and programmed sweeping frequency operation for fast profile diagnosis during a single plasma discharge. In addition, the SoC approach can help millimeter-wave diagnostics survive the harsh high-radiation reactor environment by significantly improving noise rejection, system stability, and circuit protection.

For the new generation of ECE Imaging system, commercially available monolithic microwave integrated circuits (MMICs), including system-on-chip mm-wave heterodyne receivers, are integrated on LCP and housed in

[a)]Published as part of the Proceedings of the 22nd Topical Conference on High-Temperature Plasma Diagnostics (HTPD 2018) in San Diego, California, USA.
[b)]Author to whom correspondence should be addressed: amzhu@ucdavis.edu

fully shielded antenna modules designed at UC Davis in 2017. The operating frequency range of these commercial E-band receiver chips (intended for point-to-point wireless communications) is limited from 72 to 81 GHz (instead of the full 60 – 90 GHz of E-band), which is suitable for the DIII-D pedestal region ELM imaging measurements during operation under toroidal magnetic fields from 1.7 to 1.8 T. Beyond this proof-of-principle demonstration, the UC Davis microwave diagnostic team is working on new W-band (75-110 GHz) and F-band (90-140 GHz) chips for state-of-art ECE Imaging systems, which are better suited for fusion plasma diagnostics. The LCP ECE Imaging system is used as a high temporal, high spatial, high temperature resolution diagnostic for absolute 2D electron temperature profile and evolution measurement, and precursor structure imaging. The electron temperature profile recovery between ELM bursts is shown later in this paper. In Section II, we describe the upgrade details of the new ECE Imaging receiver. Section III shows the new ECE Imaging system application and observation result on DIII-D. Finally, Section IV presents the roadmap and milestones of the new millimeter-wave imaging technologies for fusion plasmas.

II. LCP ECE Imaging system application on DIII-D

The Liquid Crystal Polymer modules are successfully installed in the ECE Imaging system on DIII-D located the at 270 R-0 port for pedestal region electron temperature measurement. The receiver employs gallium arsenide (GaAs) MMICs, which give low noise temperature (865 Kelvin SSB) and high gain performance (>20 dB). On the system level, it employs liquid crystal polymer as the integration substrate with outstanding electrical and mechanical properties. The LCP modules are each designed with one MMIC on a custom PCB in an individual module box with a waveguide horn type mouth for millimeter-wave receiving, as shown in Figure 1. There is an LNA between the receiver antenna and the balanced Schottky diode mixer, which is important to amplify the ECE signal to achieve much lower noise temperature[13,14]. The horn shielding box was designed with a horn open mouth to optimize the antenna pattern. As shown in Fig. 2, the depth of the horn is 70 mm, which gives a far-field pattern comparable to that of a Gaussian beam in the working frequency range. The Gaussian beam parameters are shown in Table I.

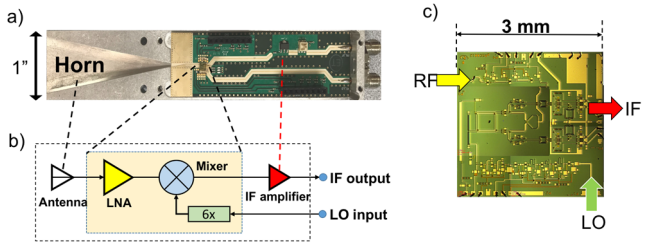

Fig.1. (a) The side view of the LCP module shows the entire printed circuit board which was installed in the individual shielding module. The input mouth is designed as a waveguide horn to achieve higher gain in the main lobe of the receiver antenna. (b) Schematic of LCP electronics including PCB layer and MMIC layer. (c) Photo of the MMIC shows the RF and LO inputs and IF output signal. The LO signal is generated by an input microwave signal and internal LO 6x multiplier chain.

TABLE I. Horn shielding box far-field pattern fitting with Gaussian beam

E-plane beamwidth	E-plane waist	H-plane beamwidth	H-plane waist
8.6 degree	9.979 mm	16.8 degree	5.108 mm

Noise temperature measurements of three of the horn-waveguide receiver modules were conducted using standard hot-cold calibration techniques. A large aperture (20 cm) NPL load was employed which is rated for measurements from 50 GHz to 20 THz and operates up to 600 C. Noise temperature of ~ 3,000 Kelvin were obtained. Unfortunately, we were not able to conduct an overall system calibration which would necessitate placing the hot-cold load inside the DIII-D vessel but hope to be permitted during the next venting. Conversion gain was determined using coherent millimeter wave illumination from a calibrated source.

Twenty individual LCP modules were mounted in two parallel arrays in a shielding enclosure box, as shown in Fig. 2. There is only one full height aperture on the front panel for ECE signal input from the plasma greatly simplifying the shielding problem. A dichroic plate with 72 GHz cutoff frequency is used to isolate noise below 72 GHz for single-band mixing on all 20 modules. It also improves the enclosure box shielding performance. The integration of the receiver enclosure box is greatly increased. In addition, all 20 individual LCP modules may be replaced independently, resulting in easier and more flexible maintenance. Since the LO multiplier signal for all 20 channels is introduced using microwave cable, there is no longer quasi-Gaussian LO beam coupling, which significantly increases LO coupling stability, removes a noise input channel, and saves free space around the tokamak device, which is very important to build highly integrated diagnostics for future fusion reactors.

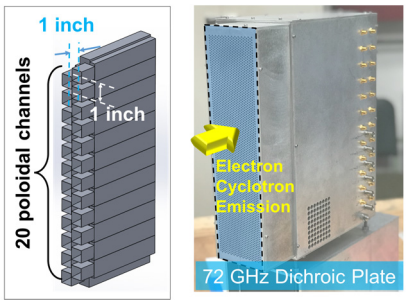

Fig. 2. There are 20 individual LCP modules installed in the shielding enclosure box with one 72 GHz dichroic plate on the front panel.

The LCP receiving optics system retains the zoom lenses from the previous ECEI optics system. All of the remaining components in the focus box have been replaced with a new cylindrical lenses, including a new H-plane lens, a new focus lens, a H2 lens, and a new reflection mirror. The image plane can cover a radial region rho from 0.99 to 0.20. The new optics system gives 1:1.25 zoom from the receiver side to the plasma side. The poloidal resolution is 12.54 mm in plasma.

III. DIII-D ECE Imaging application and result

The new LCP ECE Imaging module has only ~ 3,000 Kelvin noise temperature, which facilitates absolute electron temperature measurements in the plasma. The ECE Imaging system was employed for pedestal top region measurement in shot 175432. The radial observation window extends from rho ~ 0.37 to rho ~ 0.87, which covers the top of pedestal region as shown in Fig. 3a. The optical thick assumption is well satisfied in this radial region, which means the receiving emission temperature equals the electron temperature. With this assumption, the absolute temperature calibration is performed with the ECE Imaging signal. This is done using the electron temperature profile provided by the Thomson scattering diagnostic. The calibration coefficient is defined as the electron temperature divided by the ECE Imaging signal, with units in keV per Volt, as shown in Eqn. (1). The relationship between electron temperature and receiving signal is linear since the black body emission assumption is well satisfied. The linear fitting provides an absolute electron temperature relative calibration by Thomson scattering[15]. All channels were located at certain positions with optics alignment setup and magnetic field configuration. The linear fitting gives absolute electron temperature relative calibration by Thomson scattering, as shown in Fig. 3b.

$$cc_{i,j} = \frac{T_e(i,j)}{V_{ECEI}(i,j)} \quad (1)$$

The calibration coefficient is marked as "cc". T_e means electron temperature measured by Thomson Scattering system. Here, V_{ECEI} stands for the voltage of specified channel in the ECE Imaging 2D array. The footnote i and j are used for marking channel numbers in the poloidal and radial directions.

Following the absolute temperature calibration work, the LCP ECE Imaging system is able to generate 2D electron temperature profiles in the plasma, especially for the optically thick region. The ECE Imaging radial coverage will move outward under higher toroidal magnetic field operation. Thus, there will be some channels located in optically grey or thin regions, where density fluctuations will affect the emission temperature. It is therefore necessary to employ synthetic ECE Imaging analysis to model and fit electron temperature profiles and fluctuations[16,17]. All ECE Imaging channels have been calibrated with the Thomson Scattering system on DIII-D. The absolute electron temperature comparison result between the Thomson scattering system and LCP ECE Imaging is shown in Fig. 4a. The blue and red curves match perfectly, which means the calibration coefficient is constant. The 2D electron temperature could be captured by the LCP ECE Imaging system with reliable calibration coefficients. By zooming in on a 100-millisecond window, the LCP ECE Imaging temperature measurement shows much higher temporal resolution (~ 1 microsecond) compared to the Thomson scattering diagnostic. ECE Imaging is able to monitor temperature recovery between two ELM crashes. As shown in Fig. 5, the 1D and 2D absolute temperature profiles had been captured by LCP ECE Imaging system. Since ECE Imaging system is able to measure the absolute temperature, the temperature changes during the inter-ELM period had been captured, as shown in Fig 6. The electron temperature has sharply drop from pedestal to core with different depths during ELM crash. The temperature profile drops more on outer channels, which means the gradient of temperature will during ELM crash time. And temperature recovery processing will flat the profile from core to top of pedestal region, as shown in Fig 6b.

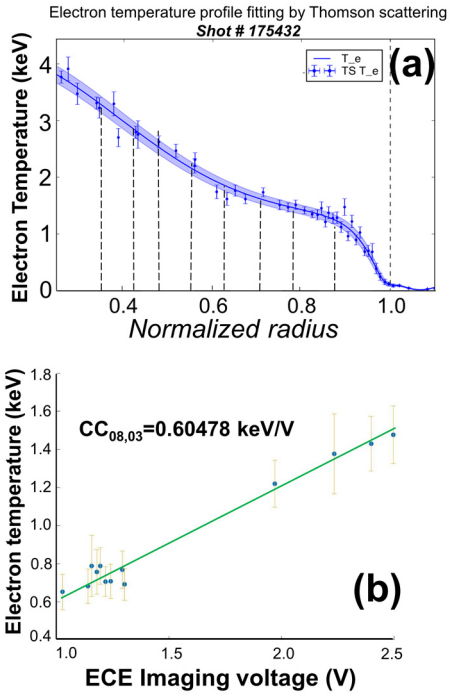

Fig. 3. (a) The blue curve stands for the temperature profile fitting with Thomson scattering data at 2080 milliseconds in shot 175432. The black dash lines mark 8 radial channels' positions of the ECE Imaging system. (b) The X-axis is the ECE Imaging specified channel voltage values. For example, the 8th poloidal channel and the 3rd radial channel have been chosen which are located at the rho ~ 0.70 flux surface. The Y-axis is the electron temperature at the same flux surface measured by Thomson scattering. The linear fitting result shows the calibration coefficient value for this channel.

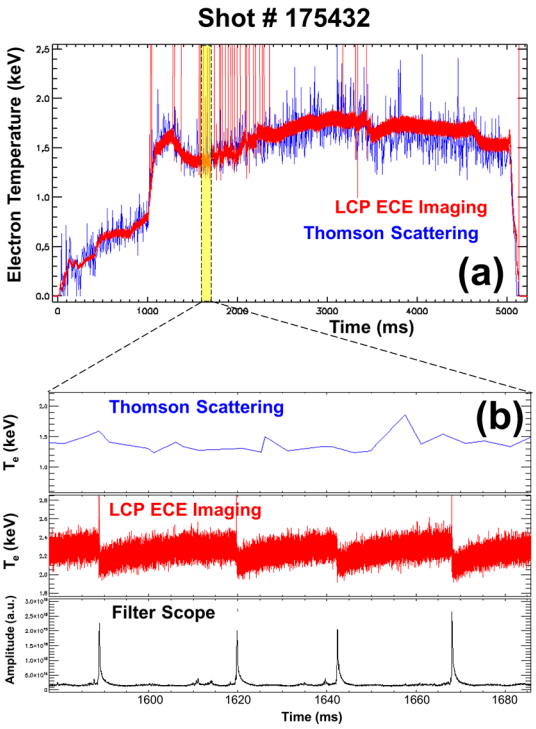

Fig. 4. (a) Comparison result between Thomson scattering and LCP ECE Imaging. The blue curve is the electron temperature from Thomson scattering CH 31, which is measured at the rho ~ 0.7 flux surface. The red curve is the calculated electron temperature by ECE Imaging (LFS0803, poloidal CH #8, radial CH #3), which is measured at the same flux surface. There is a 10-microsecond smoothing box on the ECE Imaging raw data. (b). The blue curve on the top is the electron temperature at the rho ~ 0.7 flux surface provided by Thomson scattering. The red curve stands for the high temporal resolution LCP ECE Imaging measurement, which makes obvious that temperature recovery. The black curve in the bottom subplot is filter scope data to mark ELM bursting times.

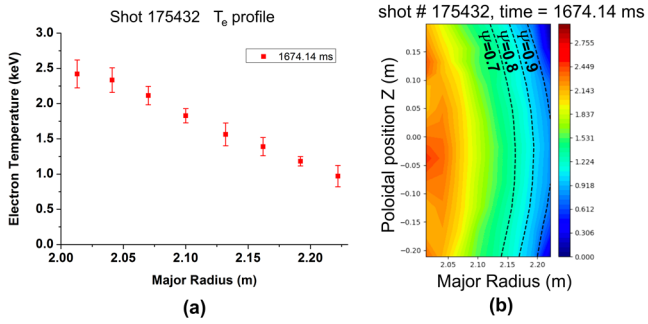

Fig 5. (a) One dimensional electron temperature measured by ECE Imaging. (b) Two dimensional electron temperature measured by ECE Imaging.

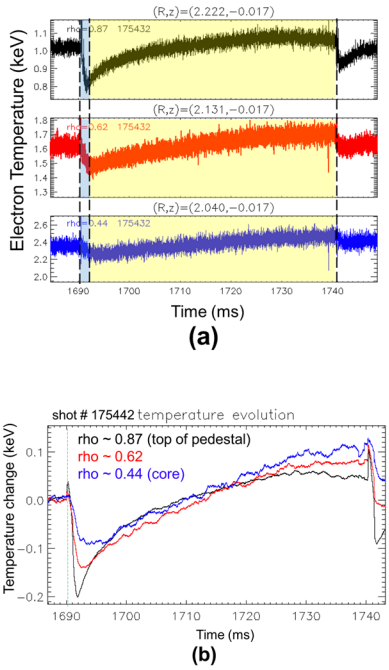

Fig. 6. (a) The raw data flow for three different radial channels on the middle plane. The temperature dropping and recovery are shown in bright and yellow boxes. (b) The temperature changes on the three different channels (with 5kHz low pass filter).

With the new enclosure box and individual module housings, the shielding performance has been significantly improved to shield the receiver from out-of-band noise. Two generations of ECE Imaging receivers were installed together for simultaneous and co-located measurements to directly compare the performance, as shown in Fig. 7. Both in-band and out-of-band noise impinges on both receivers. The signal differences directly demonstrate the outstanding shielding performance of the new LCP approach since the out-of-band interference has essentially been eliminated.

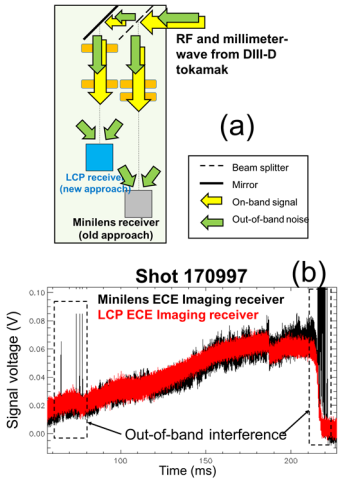

Fig. 7. (a) Experimental setup for old mini-lens and new LCP receiver simultaneous and co-located measurement comparisons. (b) Both the old mini-lens (black) and new LCP (red) instruments are used to measure the 77.7 GHz ECE signal from the DIII-D tokamak. The black spikes in the

dashed boxes show the out-of-band interference that is eliminated in the new data (red).

IV. Summary and future plan

For the initial proof-of-principle studies, commercial low-noise GaAs receiver chip modules have been successfully employed in the DIII-D upgraded ECE Imaging system. Both absolute temperature calibration and profile recovery monitoring were achieved in the FY18 campaigns. The new generation of LCP module array is able to provide valuable data for ITER baseline experiments with on-axis toroidal magnetic field of ~ 1.7 T including ELM bursting and inter-ELM physics study, QH-mode development, and advanced tokamak scenarios. Both W-band (75-110 GHz) and F-band (90 -140 GHz) custom MMICs are under development by UC Davis, which will provide higher operation frequency and much wider bandwidth. The resultant frequency ranges are shown in Fig. 8. The ECE Imaging system is able to apply for 2D non-locate heat propagation and absolute temperature imaging in both the pedestal and core regions.

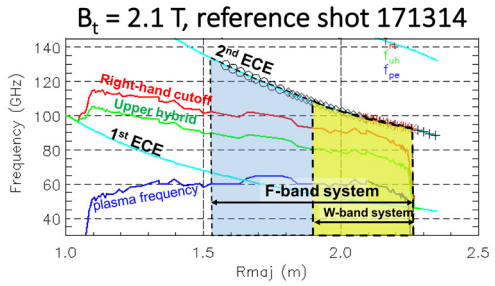

Fig. 8. Characteristic microwave frequencies in plasma under 2.1 T on-axis toroidal magnetic field. The W-band and F-band LCP ECE Imaging system is able to cover rho ~ [-0.17, 0.99] region in the plasma.

V. Acknowledgements

This work is supported in part by US DoE under US DoE grants DE-AC02- 09CH11466, DE-FG02-99ER54531 and DE-FC02-04ER54698. Thanks for the support of DIII-D Thomson scattering diagnostic team.

VI. DISCLAIMER

VII. REFERENCES

[1]Tobias, B., Kong, X., Liang, T., Spear, A., Domier, C.W., Luhmann Jr, N.C., Classen, I.G.J., Boom, J.E., Van De Pol, M.J., Jaspers, R. and Donné, A.J.H., Review of Scientific Instruments, 80(9), p.093502.(2009)
[2]Choi, M.J., Yun, G.S., Lee, W., Park, H.K., Park, Y.S., Sabbagh, S.A., Gibson, K.J., Bowman, C., Domier, C.W., Luhmann Jr, N.C. and Bak, J.G., Nuclear Fusion, 54(8), p.083010.(2014)
[3]Deng, B.H., Domier, C.W., Luhmann Jr, N.C., Donné, A.J.H. and Van De Pol, M.J., Review of Scientific Instruments, 72(1), pp.368-370.(2001)
[4]Zhu, Y.L., Xie, J.L., Yu, C.X., Zhao, Z.L., Gao, B.X., Chen, D.X., Liu, W.D., Liao, W., Qu, C.M., Luo, C. and Hu, X., Review of Scientific Instruments, 87(11), p.11D901.(2016)
[5]Jiang, M., Shi, Z.B., Che, S., Domier, C.W., Luhmann Jr, N.C., Hu, X., Spear, A., Liu, Z.T., Ding, X.T., Li, J. and Zhong, W.L., Review of Scientific Instruments, 84(11), p.113501.(2013)
[6]Pan, X.M., Yang, Z.J., Ma, X.D., Zhu, Y.L., Luhmann Jr, N.C., Domier, C.W., Ruan, B.W. and Zhuang, GReview of Scientific Instruments, 87(11), p.11E106.(2016)
[7]Tobias, B., Domier, C.W., Liang, T., Kong, X., Yu, L., Yun, G.S., Park, H.K., Classen, I.J., Boom, J.E., Donné, A.J.H. and Munsat, T., Review of Scientific Instruments, 81(10), p.10D928.(2010)
[8]Tobias, B.J., Domier, C.W., Luhmann, N.C., Boom, J.E., Classen, I.G.J., Donne, A.J.H., Yun, G., Park, H.K. and Nazikian, R.M., IEEE Transactions on Plasma Science, 39(11), pp.3022-3023. (2011).
[9]Tobias, B.J., Classen, I.G.J., Domier, C.W., Heidbrink, W.W., Luhmann Jr, N.C., Nazikian, R., Park, H.K., Spong, D.A. and Van Zeeland, M.A., Physical review letters, 106(7), p.075003.(2011)
[10]Classen, I.G.J., Westerhof, E., Domier, C.W., Donné, A.J.H., Jaspers, R.J.E., Luhmann Jr, N.C., Oosterbeek, J.W. and Park, H.K., In Proc. 14th Joint Workshop Electron Cyclotron Emission and Electron Cyclotron Resonance Heating (pp. 9-12). (2006)
[11]Yun, G.S., Lee, W., Choi, M.J., Lee, J., Park, H.K., Tobias, B., Domier, C.W., Luhmann Jr, N.C., Donné, A.J.H., Lee, J.H. and KSTAR Team, Physical review letters, 107(4), p.045004. (2011)
[12]Wang, Y., Tobias, B., Chang, Y.T., Yu, J.H., Li, M., Hu, F., Chen, M., Mamidanna, M., Phan, T., Pham, A.V. and Gu, J., Nuclear Fusion, 57(7), p.072007.(2017)
[13]Lai, J., Domier, C.W. and Luhmann Jr, N.C., Review of Scientific Instruments, 85(3), p.033501.(2014)
[14]Tobias, B., Domier, C.W., Luhmann Jr, N.C., Luo, C., Mamidanna, M., Phan, T., Pham, A.V. and Wang, Y., Review of Scientific Instruments, 87(11), p.11E103.(2016)
[15]Carlstrom, T.N., Campbell, G.L., DeBoo, J.C., Evanko, R., Evans, J., Greenfield, C.M., Haskovec, J., Hsieh, C.L., McKee, E., Snider, R.T. and Stockdale, R., Review of Scientific Instruments, 63(10), pp.4901-4906. (1992)
[16]Shi, L., Valeo, E.J., Tobias, B.J., Kramer, G.J., Hausammann, L., Tang, W.M. and Chen, M., Review of Scientific Instruments, 87(11), p.11D303. (2016)
[17] M. Chen, Y. Zhu, L. Shi, C. Luo, B, Tobias, N.C. Luhmann. Review of scientific instruments (HTPD 2018 conference, San Diego) (submitted)(2018)